DEPARTMENT OF MECHANICAL ENGINEERING
COLLEGE OF ENGINEERING & TECHNOLOGY
OLD DOMINION UNIVERSITY
NORFOLK, VIRGINIA 23529

AERODYNAMIC SHAPE OPTIMIZATION OF A HSCT TYPE CONFIGURATION WITH IMPROVED SURFACE DEFINITION

By

A.M. Thomas

and

Surendra N.Tiwari, Principal Investigator

Progress Report
For the period ended June 30, 1994

October 1994

FOREWORD

This is a progress report on the research project "Surface Modeling and Optimization Studies of Aerodynamic Configurations". Within the guidelines of the project, special attention was directed toward research activities in the area of "Aerodynamic Shape Optimization of a HSCT Type Configuration With Improved Surface Definition". The period of performance of this specific research was May 1, 1993 through June 30, 1994.

ABSTRACT

AERODYNAMIC SHAPE OPTIMIZATION OF A HSCT TYPE CONFIGURATION WITH IMPROVED SURFACE DEFINITION

Almuttil M. Thomas[†]

Surendra N. Tiwari[§]

Two distinct parametrization procedures of generating free-form surfaces to represent aerospace-vehicles are presented. The first procedure is the representation using spline functions such as Non-Uniform Rational B-Splines (NURBS) and the second is a novel (geometrical) parametrization using solutions to a suitably chosen partial differential equation. The main idea is to develop a surface which is more versatile and can be used in an optimization process. Unstructured volume grid is generated by an advancing front algorithm and solutions obtained using an Euler solver. Grid sensitivity with respect to surface design parameters and aerodynamic sensitivity coefficients based on potential flow is obtained using an Automatic Differentiator precompiler software tool. Aerodynamic shape optimization of a complete aircraft with twenty four design variables is performed. High speed civil transport aircraft (HSCT) configurations are targeted to demonstrate the process.

† Graduate Research Assistant, Department of Mechanical Engineering, Old Dominion University, Norfolk, VA 23529–0247.

§ Eminent Professor, Department of Mechanical Engineering, Old Dominion University, Norfolk, VA 23529–0247.

TABLE OF CONTENTS

1. INTRODUCTION

The design of aerospace vehicles requires the solution of mathematical models to represent surfaces which are systems of either algebraic, differential or integral equations [1]. The defining characteristic of these surfaces is that they must be changeable by the designer. The use of rational polynomial functions for representing curves and surfaces in CAD/CAM applications is becoming increasingly important.

The type of polynomial functions used gives various forms of curves and surface representations, for example, coons patch, Bezier curves and surfaces, B-splines, and rational B-splines. Free-form surface design using such curve and surface representations has been discussed by a number of authors. The method of using rational B-spline curve to produce a variety of different surface shapes is described by Tiller [3–4]. Woodard [5] presents a variety of techniques for producing free form surfaces and goes on to describe, in some detail, interactive skinning technique using B-spline surface interpolation. The increasing popularity of rational Bezier and B-spline forms is due to the fact that they offer one common mathematical form for precise representation of standard analytical shapes such as lines, conics, circles, planes and quadric surfaces [6].

Free form surfaces can also be generated as a solution to a suitably chosen Partial Differential Equation (PDE), and this has been investigated by Bloor and Wilson [7–9]. The method uses PDEs as a means of producing blend surfaces. By regarding blend as a solution to a boundary-value problem and by choosing appropriate boundary conditions, it was demonstrated that a solution to an elliptic PDE gave a smooth blended surface that has the required degree of continuity with the surface to which it joined. The surfaces generated by this method are expressed parametrically, often in terms of transcendental functions of the surface parameters rather than simple polynomial expressions, and hence the resulting surfaces tend to be smooth.

1

Both of the above described methods have been successfully applied to various types of surface shapes but there has been relatively little work published on the use of these forms for design of aerospace vehicles. The main goal of this study is to focus on developing surfaces for aerospace vehicles using NURBS and PDE which can be later used to compute computational grids in a very rapid manner. The ultimate goal is to produce surface and grids suitable to optimize designs in conjunction with the numerical simulation of the physics.

Grids are generated to discretize the solution domains of the physical-mathematical models so that numerical solutions can be obtained. A grid is defined as a set of points with appropriate connections between the points. The points act as reference positions within the field at which the flow variables are to be computed and the connections between the points act as pathways for transferring information around the computational domain. In a structured grid the connectivity between the points is implicitly defined through a curvilinear coordinate system. In an unstructured grid, the connectivity is arbitrary and therefore must be explicitly specified. Solution methods that utilize a structured grid are generally more efficient than methods that utilize an unstructured grid. However unstructured grids provide a much greater degree of flexibility than is available with a structured grid. In particular, unstructured grids can discretize a highly complex domain easily and are suitable for performing localized grid enrichment for solution adaptation. In this study unstructured grids around various surfaces considered are generated using the advancing front technique [10]. This method was selected because it does not require a separate library of modules to distribute grid points throughout the domain in advance like the Delauny triangulation.

Discussion on engineering design, surface modelling and grid generation technique are briefly presented. This is followed by governing equations for potential flow solution and finally calculation of sensitivity terms and optimization problem is presented and discussed.

1.1 Engineering Design and Surface Parametrization

In developing mathematical models and numerical solution techniques, parameters that characterize

2

the discipline have evolved [11]. The parameters are divided into independent parameters P_{ind} and dependent parameters P_{dep}. Independent parameters characterize discipline physics and the solution domain geometry. Examples of independent parameter for aerospace vehicle are: Mach number, Reynolds number, wing sweep, mean camber, maximum wing thickness, fuel weight, chord length, and panel thickness. Independent parameters broadcast information to specify conditions in the solution domain. In the case of geometry, independent parameters define the grid and vehicle surface. Since a mathematical model in one discipline can require input from other disciplines, this input may be classified under physics parameter. Dependent parameters are usually integration of dependent variables in mathematical models. Examples are lift, drag, weight, and wing volume.

For an aerospace vehicle such as High-Speed Civil Transport (HSCT) the traditional approach to design is for aerodynamics and performance disciplines to initially create the vehicle surface [12]. The process is to define the planform, wing, fuselage, engine nacelles, and major control surfaces with aero/performance independent-design parameters. Approximately 50–100 independent parameters are required to specify a rough vehicle surface design. Usually a sparse set of points on component surfaces which can be thought of as a coarse grid becomes the surface description for analyses. In the CAD process a considerable amount of information is added which is not provided by the low-level analyses. These additions are in the form of point movements and point creations to achieve desirable surface characteristics such as smoothness and blending of one component into another. These two aspects are kept in mind in developing surfaces for the different geometries considered here.

2. SURFACE MODELLING AND GRID GENERATION

Two different approaches have evolved in the development of parametric curves and surfaces. They are referred to here as "interpolative" and "approximative". In an interpolative representation, points and derivatives on the curve or surface are used to control the formula defining the curve and surface. Lagrangian and Hermite interpolation formulas are examples of this approach. In an approximative approach, points not necessarily on the curve or surface control the formula defining the curve or surface. Bezier and B-spline representations are examples of this approach. In the design process using an interactive CAD system, the approximative approach is highly advantageous. The basic formulation of this approach is presented here.

2.1 Rational B-Spline Curves and Surfaces

A NURBS curve [4] is a vector valued piecewise rational polynomial function of the form

$$Q(u) = \frac{\sum\limits_{i=0}^{n} \omega_i V_i B_{i,k}(u)}{\sum\limits_{i=0}^{n} \omega_i B_{i,k}(u)} \tag{2.1}$$

where ω_i are called the weights, the V_i are the control points and $B_{i,k}(u)$ are the normalized B-spline basis functions of degree k defined as

$$B_{i,0}(u) = \{ \begin{matrix} 1 & if \ u_i \le u < u_{i+1} \\ 0 & otherwise \end{matrix} \tag{2.2}$$

$$\begin{aligned} B_{i,k}(u) &= \frac{u - u_i}{u_{i+k} - u_i} B_{i,k-1}(u) \\ &+ \frac{u_{i+k+1} - u}{u_{i+k+1} - u_{i+1}} B_{i+1,p-1}(u) \end{aligned} \tag{2.3}$$

where u_i are the so-called non-uniform knots forming a knot vector.

4

An interactive program based on the formulation given by Eqs. (2.1) – (2.3) has been developed. In this program, after prescribing an initial set of control points, the designer can pick and drag these points and simultaneously observe the change in the shape of the curve. Weights can also be specified at each control points and the curve can be modified. As a simple example, this approach is applied to the design of cambered airfoils. The airfoil is controlled directly with NURBS control points and weights. Figure 2.1 shows a six control point definition of the cambered airfoil. The points at the leading edge and trailing edge are fixed. Two control points at 0% chord are used to affect the bluntness of the section. The effect of the movement of the control points to create another airfoil is shown in Fig. 2.2. Figure 2.3 shows the effect of increasing the weight of the middle control point. It is seen that the curve is pulled towards the control point. An arc length based discretization of the unit line is used for the knot vector.

A NURBS surface [6] is the rational generalization of the tensor product nonrational B-spline surface and is defined as

$$S(u,v) = \frac{\sum\limits_{i=0}^{n}\sum\limits_{j=0}^{m} \omega_{i,j}\, V_{i,j}\, B_{i,k}(u)B_{j,q}(v)}{\sum\limits_{i=0}^{n}\sum\limits_{j=0}^{m} \omega_{i,j}\, B_{i,k}(u)B_{j,q}(v)} \qquad (2.4)$$

where $\omega_{i,j}$ are the weights, $V_{i,j}$ form a control net, and $B_{i,k}(u)$ and $B_{j,q}(v)$ are the normalized B-splines of degree k and q in the u and v directions, respectively. The knot vectors are

$$U = \{0,0,...0,u_{k+1},...,u_{r-k-1},1,1,...1\}$$

$$V = \{0,0,...0,u_{q+1},...,u_{s-q-1},1,1,...1\}$$

where the end knots are repeated with multiplicities $k+1$ and $q+1$ and $r = n + k + 1$ and $s = m + q + 1$.

A NURBS surface has the property $\sum\limits_{i=0}^{n}\sum\limits_{j=0}^{m} B_{i,k}(u)B_{j,q}(v) = 1$ and reverts to a B-spline when all the weights are 1. It has the advantage of being able to represent free form surfaces, and with the proper choice of weights, conic surfaces. Surface skinning technique [5] is used to obtain the NURBS surface. The task of skinning is to fit a surface through an ordered set of space curves, called as section curves. The positioning of section curves in the three-dimensional space is customarily done with respect to a

spline curve, from which appropriate orientation vectors can be automatically computed. The surface skinning technique is used to define NURBS surface. An ONERA M6 wing is used for this case. The wing has a leading edge sweep of 30 degrees, an aspect ratio of 3.8, taper ratio of 0.56, and symmetrical airfoil sections. The wing defined by three wing sections and nine control points per section is shown in Fig. 2.4. The NURBS surface generated using these control points is shown in Fig. 2.5.

2.2 The PDE Method

The PDE method generates a surface $\underline{X}$ in Euclidean 3–space, which is a function of two parameters, i.e., $\underline{X}$ = (x(u,v), y(u,v), z(u,v)). The surface is obtained by solving a partial differential equation (PDE), in parameter u,v space, subject to boundary condition on $\underline{X}$ and its normal derivative with respect to u and v. In general the order of PDE determines the number of derivatives of the unknown function that must be specified in the boundary condition. If control over both shapes of the curves bounding the PDE surface patch and the directions and magnitude of the coordinate vectors $\underline{X}_u$ and $\underline{X}_v$ at the edge of the patch are required then atleast a fourth order PDE is needed to generate the surface. The PDE may be written as

$$\left[\frac{\partial^2}{\partial u^2} + a^2 \frac{\partial^2}{\partial v^2} \right]^2 \mathbf{\underline{X}} = 0 \qquad (2.5)$$

where $\underline{X}$ = (x(u,v), y(u,v), z(u,v)).

The appropriate boundary conditions for Eq. (2.5) is the value of $\underline{X}$ and its normal derivative around the edges of the domain in the (u,v) plane. Since the generating Eq. (2.5) is an elliptic PDE, the solution becomes very sensitive to the choice of boundary conditions. The boundary conditions act as a powerful tool for surface manipulation by a designer and can be used as a design parameter in an optimization process. The boundary conditions on function $\underline{X}$ are so chosen that the curves forming the edges of the surface patch have the designed shape. The directions of the vector $\underline{X}_u$ and $\underline{X}_v$ are tangential to the isoparametric lines on the surface. Therefore by altering the values specified for $\underline{X}_u$ and $\underline{X}_v$ along the boundaries one can effect the direction in which the surface moves away from the edges of the patch.
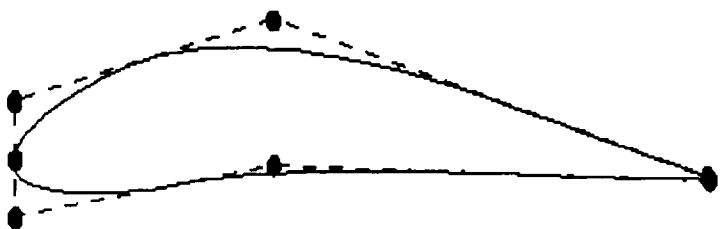
6

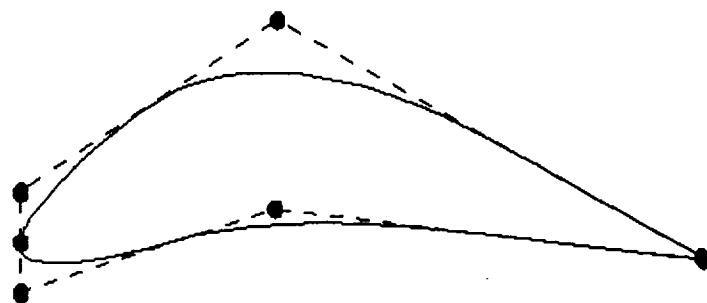**Fig. 2.1 Six control points NURBS wing section.**

Fig. 2.2 Effect of control point movement.
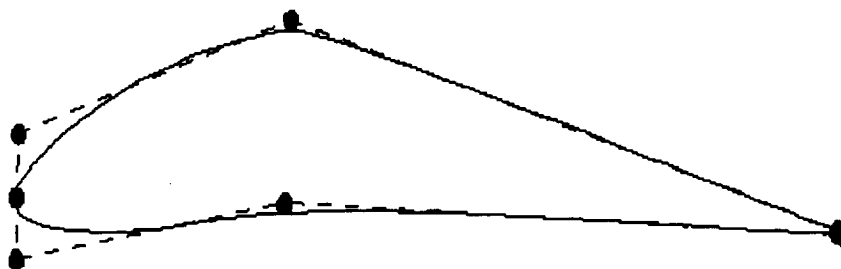

Fig. 2.3 Effect of increasing the weight of a control point.
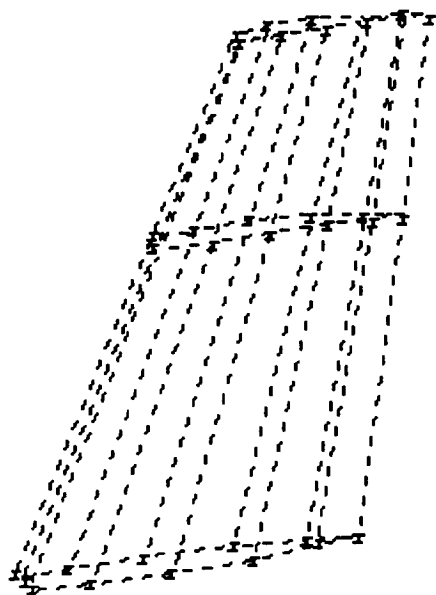
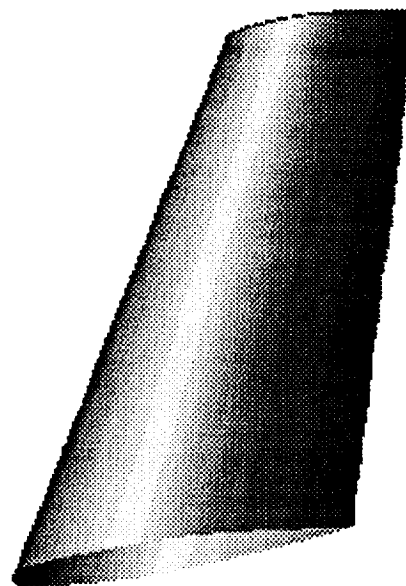

Fig.2.4 Control point mesh for an M6 wing.

Fig. 2.5 NURBS surface for an M6 wing.

7

The general solution of Eq. (2.5) can be written in the form

$$\underline{X} = A_0(u) + \sum_{n=1}^{\infty}(A_n(u)\cos(nv) + B_n(u)\sin(anv))$$

where the coefficient function $A_n(u)$ and $B_n(v)$ are of the form

$$A_n(u) = a_{n1}e^{anu} + a_{n2}ue^{anu} + a_{n3}e^{-anu} + a_{n4}ue^{-anu}$$

$$B_n(v) = b_{n1}e^{nv} + b_{n2}ve^{nv} + b_{n3}e^{-nv} + b_{n4}ve^{-nv}$$

and a_{n1}, a_{n2}, a_{n3}, a_{n4}, b_{n1}, b_{n2}, b_{n3}, b_{n4} are vector valued constants that can be found for a particular solution by Fourier analysis of the condition imposed on the isoparametric lines bounding the patch. Now consider the generation of PDE surfaces for the HSCT configuration. It is necessary to set up the problem as a boundary value problem in (u,v) space, with boundary condition specified along curves in the (u,v) plane. One of the boundary curve is taken to be the plan outline of the intersection of the wing and the fuselage. On this curve, u is taken to be zero and the shape is given parametrically in terms of v. Another boundary curve is taken to be u=1 and again is given parametrically in terms of v. This curve is an airfoil section at the mid portion of the double delta wing. The whole wing is generated as two separate sections and the fuselage is represented as a Fourier series

Families of wing sections are described by combining a mean line and a thickness distribution. The resultant expression possesses the necessary features that suit the problem, mainly the concise description of a wing section in terms of several design parameters. The design parameters are: M = the maximum ordinate of the mean line or camber, and C = chordwise position of maximum ordinate. The thickness distribution is a bit different from the regular NACA four-digit wing section representation. Here the design parameters are T = The maximum thickness, P1 = first Fourier wing shape parameter, and P2 = second Fourier wing shape parameter. The ξ – coordinate is first mapped into the chord line $\bar{x} = \bar{x}(r) = \bar{x}(f_1(\xi))$ forward and the reversed to cover both the top and bottom of the section. The

8

mean line equation is

$$\bar{y}_c(\bar{x}) = \frac{\mathbf{M}}{\mathbf{C}^2}\left(2\mathbf{C}\bar{x} - \bar{x}^2\right), \quad \bar{x} \le \mathbf{C}$$

$$\bar{y}_c(\bar{x}) = \mathbf{M}\frac{\left(1 - 2\mathbf{C} + 2\mathbf{C}\bar{x} - \bar{x}^2\right)}{\left(1 - \mathbf{C}\right)^2}, \quad \bar{x} \ge \mathbf{C}$$

(2.6)

The section thickness is given by

$$y_{\mathbf{T}}(\bar{x}) = \left(-\frac{\mathbf{T}}{2}\right)(\sin(2\bar{x}) + \mathbf{P_1}\sin(4\bar{x}) + \mathbf{P_2}\sin(6\bar{x}))$$

(2.7)

The section coordinates are

$$x_l\left(r, \mathbf{P}_1^\xi\right) = \bar{x} \quad, \quad y_l\left(r, \mathbf{P}_1^\xi\right) = \bar{y}_c(\bar{x}) \pm y_{\mathbf{T}}(\bar{x})$$

The PDE surface generated is shown in Fig. 2.6 and the various parameters that define the surface are shown in Fig. 2.7.

2.3 Graphic Interface

To get a feel of how the PDE surface behaves with the change in design variables, a graphic interface software Airplane Design and Shape Parametrization (ADSP) is developed. The software is based on Forms library and runs on a Silicon Graphics machine. The design variables are represented in the form of buttons for the convenience of user. A user can select anyone of these design variables and change to see interactively the surface being changed. A separate window is provided to show the values of the design variables being changed. The program is also menu driven and the object can be represented either as shaded polygon or as wire frame. Figure 2.8 shows a snapshot of the software.

2.4 Unstructured Grid Generation and Method of Solution

VGRID3D [10] advancing front grid generation code is used to generate unstructured grids. The procedure begins by inputting points defining the surface of the geometry. The surfaces are decomposed into smaller patches (3/4–sided) and then a background grid that defines the local grid characteristics
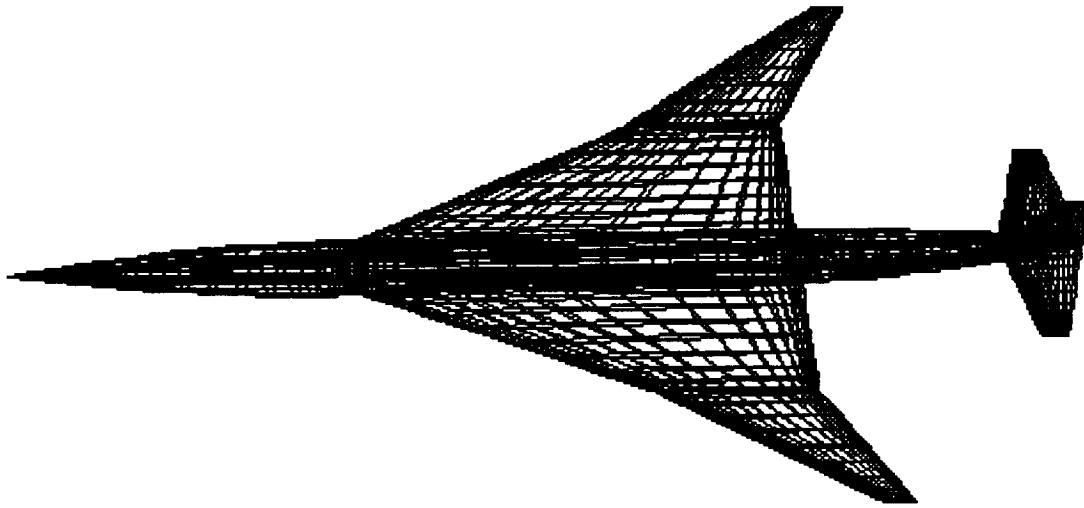
9

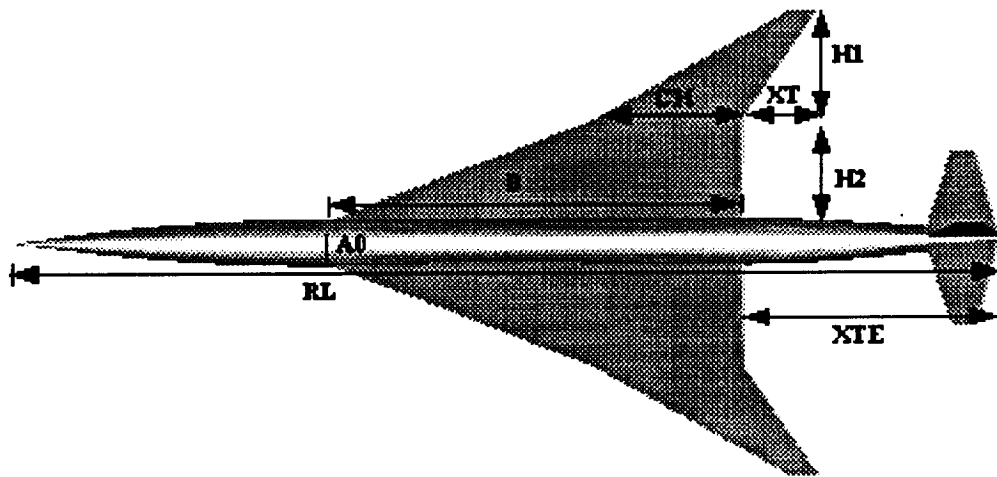**Fig. 2.6 PDE surface mesh for HSCT type configuration.**

Fig. 2.7 Surface parametrization of HSCT type configuration.

Fig. 2.8 Snapshot of the PDE graphic interface software "Airplane Design and Shape Parametrization"

such as grid spacing, stretching and stretching direction is specified. The advancing front algorithm first places points on the boundary segments that define the solution domain. This yields the initial front. Using the information stored on the background grid, the surface patches are first triangulated and this forms the interior surface triangulation. The triangulation is not on the actual NURBS or PDE surfaces, but it is close to the surface. The resulting triangulation is then projected on to the actual surface using the GRIDTOOL [13] which is then used to generate the volume grid.

The governing equations are the three-dimensional unsteady Euler equations for inviscid compressible flow. For a bounded domain Ω with a boundary $\partial\Omega$, the time dependent Euler equations in integral form can be written as :

$$\frac{\partial}{\partial t} \iiint_{\Omega} \bar{Q} \, dv \; + \; \iint_{\partial\Omega} \bar{F}(\bar{Q}) \bullet \hat{n} dS \; = \; 0 \tag{2.8}$$

where

$$\bar{Q} \; = \; \{\rho, \rho u, \rho v, \rho w, \rho e_o\}^T$$

and

$$\bar{F}(\bar{Q}) =$$

$$\left\{ \begin{array}{c} (\rho u, \rho v, \rho w) \\ (\rho u^2 + P, \rho uv, \rho uw) \\ (\rho vu, \rho v^2 + P, \rho vw) \\ (\rho wu, \rho wv, \rho w^2 + P) \\ ((\rho e_o + P)u, (\rho e_o + P)v, (\rho e_o + P)w) \end{array} \right\}$$

In the preceding equations, ρ is the density, u, v and w are the x, y, z components of the velocity, e_o is the total energy per unit volume and P is the pressure. The equations are nondimensionalized by a reference density ρ_∞ and speed of sound a_∞. Assuming an ideal gas, the pressure is written as

$$P = (\gamma - 1)\left(e_0 - \frac{1}{2}\rho(u^2 + v^2 + w^2)\right) \tag{2.9}$$

where γ represents the ratio of specific heats.

The inviscid flow field is computed on the unstructured grids using USM3D, a three–dimensional upwind flow solver developed at NASA/LaRC [14]. The spatial discretization is accomplished with a cell centered finite volume formulation using the flux difference splitting procedure. The solution is advanced in time using a three-stage Runge-Kutta time stepping scheme. Local time stepping and implicit residual smoothing are used to accelerate the convergence of the solution to a steady state.

Unstructured grid is generated around the NURBS M6 wing using the advancing front technique and is shown in Fig. 2.9. Converged solution is obtained for $M_\infty=0.84$ and $\alpha=3.06^\circ$ and the upper surface pressure contour is shown in Fig. 2.10. The figure clearly shows a double shock wave on the upper surface [15].

The surface triangulation for the HSCT type PDE surface is shown in Fig. 2.11. To simulate this HSCT configurations with engines and to study the performance features, two nozzles with square cross-section are placed just below the wings. The surface triangulation for this configuration is shown in Fig. 2.12. Both configurations are tested for $M_\infty=0.84$ and $\alpha=5^\circ$. Three stage Runge-Kutta time stepping scheme is used to obtain a converged solution. Figure 2.13 shows the shaded Cp plot for the HSCT configuration without engines. Contours are plotted by taking a cutting plane at the mid section of the configuration. A shock wave is seen at the upper surface of the wing. A total lift of 0.33358 and a drag 0.04301 were obtained. Figure 2.14 shows the Cp plot for the HSCT with engines. Similar results were obtained, but the lift was found to be 0.313434 and the drag 0.05932.
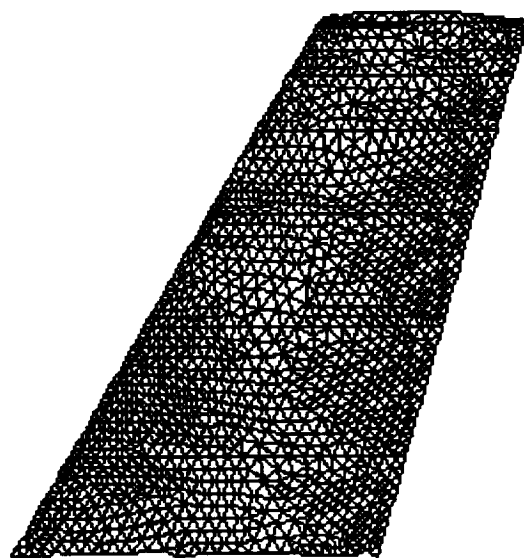
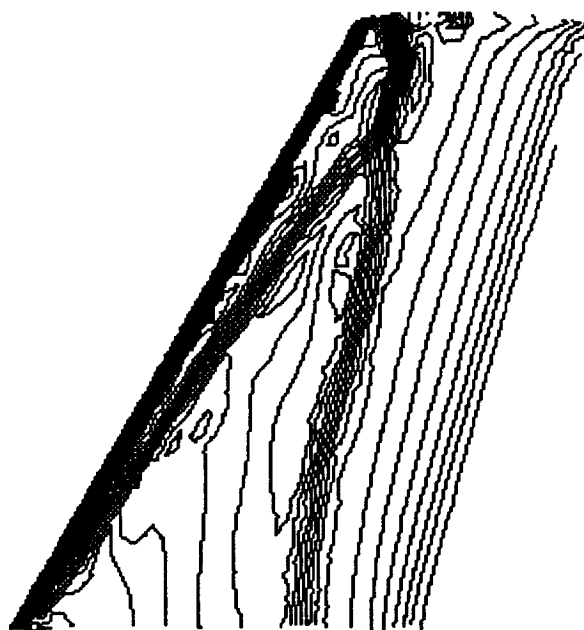**Fig. 2.9 Unstructured grid over NURBS M6 wing.**
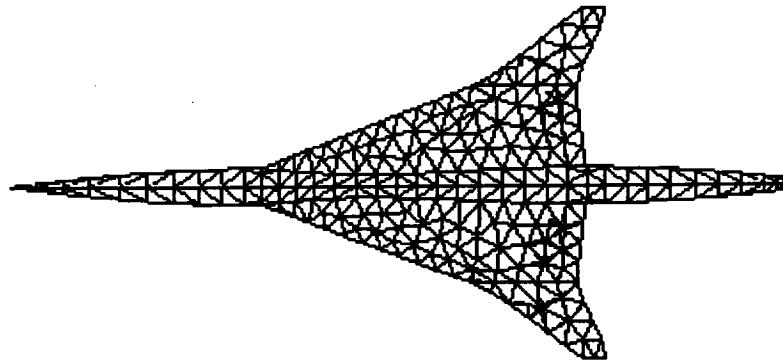

Fig. 2.10 Cp contours over M6 wing.

14
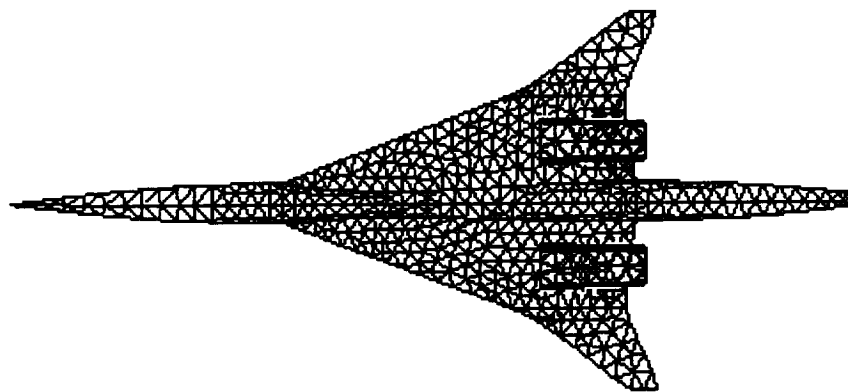
Fig. 2.11 Unstructured grid for the HSCT type configuration.

Fig. 2.12 Unstructured grid for the HSCT type configuration with engines.
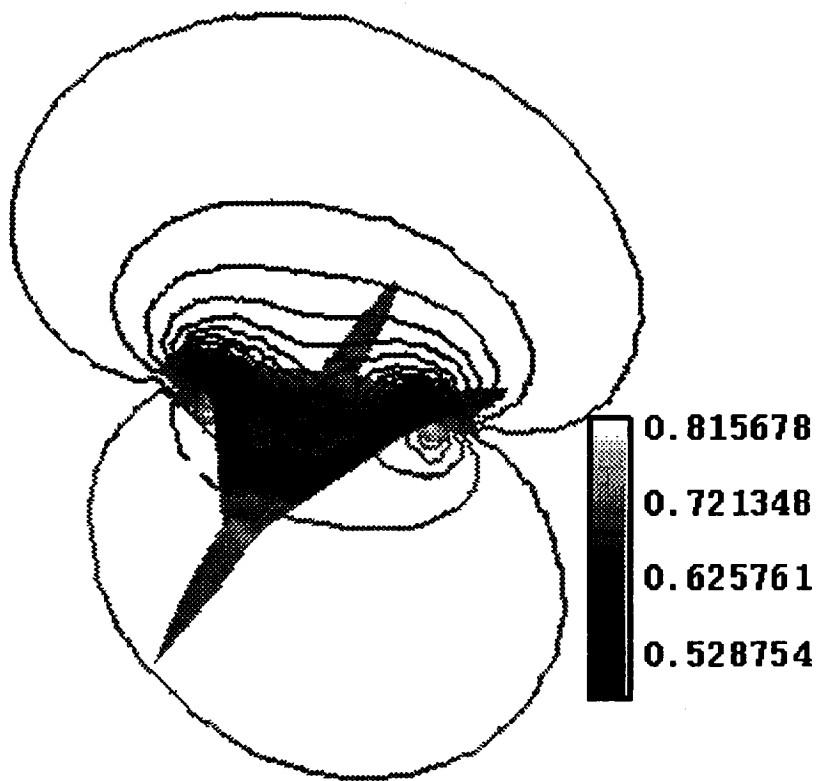
Fig. 2.13 Cp plot for the HSCT configuration without engines.

0.815678
0.721348
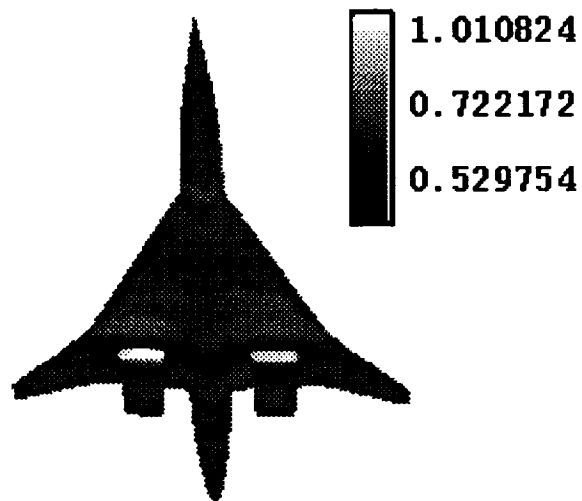0.625761
0.528754

1.010824
0.722172
0.529754

Fig. 2.14 Shaded Cp plot for the HSCT type configuration with engines.

16

3. GOVERNING EQUATIONS FOR POTENTIAL FLOW SOLUTION

A low-order potential-flow panel code for modeling complex three-dimensional geometries is used to calculate surface pressure variations. The flow field is assumed to be inviscid, irrotational and incompressible. The velocity potential is given by the Laplace's equation:

$$\nabla^2 \Phi = 0 \tag{3.1}$$

The potential at any point P may be evaluated by applying Green's Theorem which results in the following integral equation

$$\Phi_P = \frac{1}{4\pi} \iint\limits_{S+W+S_\infty} (\Phi - \Phi_i)\bar{n}.\nabla\left(\frac{1}{\bar{r}}\right)dS - \frac{1}{4\pi} \iint\limits_{S+W+S_\infty} \bar{n}(\nabla\Phi - \nabla\Phi_i)dS \tag{3.2}$$

It is assumed that the wake is thin and there is no entrainment, so the source term for the wake disappears and the jump in normal velocity across the wake is zero. Hence the simplified equation becomes

$$\Phi_P = \frac{1}{4\pi}\iint\limits_{S} (\Phi - \Phi_i)\bar{n}.\nabla\left(\frac{1}{\bar{r}}\right)dS - \frac{1}{4\pi}\iint\limits_{S} \left(\frac{1}{\bar{r}}\right)\bar{n}.(\nabla\Phi - \nabla\Phi_i)dS$$
$$+ \frac{1}{4\pi} \iint\limits_{W} (\Phi_U - \Phi_L)\bar{n}.\nabla\,\bar{n}.\nabla\left(\frac{1}{\bar{r}}\right)\left(\frac{1}{\bar{r}}\right)dS + \phi_{\infty p} \tag{3.3}$$

Dirichlet type boundary condition is used to solve Eq. (3.3). The total potential Φ can be viewed as being made up of an onset potential Φ_∞ and a perturbation potential $\phi = \Phi - \Phi_\infty$. The potential of the fictitious flow is set equal to the onset potential, ϕ_∞. With this boundary condition, the singularities on the surface tend to be smaller than if the potential of the fictitious flow is set to zero because the singularities only have to provide the perturbation potential instead of the total potential. The general equation for the potential at any point P cab be written as

$$\Phi_P = [\iint\limits_{S-P} \mu\bar{n}.\nabla\left(\frac{1}{\bar{r}}\right)dS + K\mu_p] + \iint\limits_{S} \left(\frac{\sigma}{\bar{r}}\right)dS + \iint\limits_{W} \mu_W\bar{n}.\nabla\left(\frac{1}{\bar{r}}\right)dS + \phi_{\infty p} \tag{3.4}$$

17

where K = 0 if P is not on the surface, K = 2 π if P is on a smooth part of the outer surface, and K = − 2 π if P is on a smooth part of the inner surface. If the surface is broken up into panels, Eq. (3.4) can be written in discretized form, breaking the integrals up into surface integrals over each panel. A constant strength source and doublet distribution is assumed over each panel and so the doublet and source strengths are factored out of the integrals. Taking point P to be at the centroid on the inside of one of the panels, the surface integrals over each panel are summed for all panels. For the panel containing point P, the surface integral is zero and only the $-2\pi\mu_p$ term remains in the bracketed part of Eq. (3.4). For all other panels, the surface integral is used and the $-2\pi\mu_p$ term is zero since the point P is not on the surface of any other panels. The process is repeated for point P at the centroid of every panel to yield a set of linear simultaneous equations to be solved for the unknown doublet strength on each panel. The surface integrals represent the velocity potential influence coefficients per unit singularity strength for panel K acting on the control point of panel J. Hence Eq. (3.4) becomes

$$\sum_{K=1}^{N_s} (\mu_K C_{JK}) + \sum_{K=1}^{N_s} (\sigma_K B_{JK}) + \sum_{L=1}^{N_w} (\mu_{W_L} C_{JL}) = 0 \qquad (3.5)$$

where

$$B_{JK} = \iint_K \frac{1}{\overline{r}} dS \qquad (3.6)$$

and

$$C_{JK} = \iint_K \overline{n}.\nabla\left(\frac{1}{\overline{r}}\right) dS \qquad (3.7)$$

$$C_{JJ} = -2\pi$$

The coefficients C_{JK} and B_{JK} represent the velocity potential influence coefficients per unit singularity strength for panel K acting on the control point of panel J. Equations (3.6) and (3.7) are functions of geometry only and thus can be solved for all panels to form the influence coefficient matrix. Since the source values are known, they may be transferred to the right hand side of the matrix equation. Solutions for Eqs. (3.6) and (3.7) can be found in [15].

18

4. COMPUTATION OF SENSITIVITY TERMS WITH RESPECT TO DESIGN PARAMETERS

After discretization, the steady state governing equations of the fluid flow and the boundary conditions can be expressed as

$$R(Q(D), X(D), D) = 0 \qquad (4.1)$$

where Q is the velocity potential for a potential flow and X is the computational grid or panels in the present case, and D is a vector of independent input (design) variables.

As an alternative approach a quasi-Newton iteration can be applied which can be represented as

$$-\frac{\widetilde{\partial R}}{\partial Q}\triangle Q = R^n \qquad (4.2)$$

$$Q^{n+1} = Q^n + \triangle Q \qquad (4.3)$$

Application of the quasianalytical methods that has been investigated by many researchers [16] requires the construction and evaluation of many derivatives (eg. the Jacobian matrices $\frac{\partial R}{\partial Q}$ and $\frac{\partial R}{\partial X}$). For advanced CFD codes the task of constructing exactly all of these required derivatives by hand and then building the software for evaluating these terms is extremely complex, error prone, and practically speaking, impossible. A promising possible solution to this problem may be found in the use of a technique known as automatic differentiation (AD) which has been used in the present study. The process involves the application of a precompiler software tool that automatically differentiates the application program source code from which sensitivity derivatives are to be obtained. The output of the AD precompiler procedure is a new source code which, upon compilation and execution, will compute the

19

numerical values of the derivatives of any specified output functions with respect to any specified input parameters. This AD precompiler tool has been efficiently tested by Bischof et al. [17] and Green et al. [18] in applications to an advanced CFD flow-analysis code called TLNS3D [19].

When AD is applied directly to the potential flow code, the resulting AD-enhanced code calculates the required sensitivity derivatives through an iterative process. From the discussion in [17], the process whereby sensitivity derivatives are iteratively calculated after the application of AD can be represented conceptually by combining Eq. (4.2) and (4.3) i.e., the basic CFD solution procedure, and differentiating with respect to D. The result is

$$Q'^{n+1} = Q'^{n} - P^{n}R'^{n} - P'^{n}R^{n}$$

where $P \equiv \left(\frac{\widetilde{\partial R}}{\partial Q} \right)^{-1}$.

The Automatic Differentiator (ADIFOR) procedure generates a new version of the potential flow code that has the capability to calculate the derivatives of lift, drag, and pitching moment with respect to a wide variety of different types of input parameters (including parameters related to the geometric design). Table 4.1 show the non-geometric and geometric ADIFOR sensitivity values compared with finite difference. It is seen that the results obtained by ADIFOR is in good agreement with that of the finite difference.

4.1 Grid Sensitivity with respect to Design Parameters

Typical CFD calculations are performed on a computational mesh that is "body-oriented". Changes in the geometric shape result in the movement of grid points throughout the entire mesh. One method for calculating these grid sensitivity terms is by finite differences. If forward difference approximations are selected, for example, the mesh generation code is used to produce one additional perturbed grid for a slightly perturbed value of each geometric shape design variable of interest. This procedure is generally expected to be reliable in producing accurate grid sensitivity terms because the relationships that are associated with the mesh generation process should be very smooth by design.

20

In this study, however, the precompiler tool AD (i.e., ADIFOR) is applied directly to the grid generation program to successfully calculate the grid sensitivity terms. Figures 4.1a and 4.1b show the comparison of the grid sensitivity with respect to camber between the ADIFOR and finite difference results. These grid derivatives were subsequently coupled directly to the AD-enhanced potential flow code PMARC. The final result is the successful calculation of aerodynamic sensitivity derivatives with respect to geometric design parameters.

4.2 Optimization Problem

An objective of multidisciplinary optimization of a vehicle design is to extremize a payoff function combining dependent parameters from several disciplines. Most optimization techniques require the sensitivity of the payoff function with respect to free parameters of the system. For a fixed grid and solution conditions, the only free parameter are the surface design parameters. Therefore, the sensitivity of the payoff function with respect to design parameters are needed.

The present optimization strategy is based on maximizing the lift coefficient, C_L, in response to surface perturbation, subject to pre-determined design constraints. Upper and lower bounds are set for each design parameter and the sensitivity derivatives of the objective function, $\frac{\partial C_L}{\partial X_D}$, and the constraint, $\frac{\partial C_D}{\partial X_D}$, are obtained as previously described. Throughout the analysis, the drag coefficient, C_D, is to be no greater than the value of the initial design. The strategy, illustrated in Fig. 4.2, requires that the grid and grid sensitivity derivatives be provided dynamically during the automated optimization process.

Optimization on the HSCT type configuration shown in Fig 2.6 was carried out on a SGI machine with a memory capacity of 512 MB. Sixteen design variables were selected for the optimization process. A total of twelve design optimization cycle was performed and each iteration took approximately 7.5 min of cpu time. It was seen that the lift which was initially 0.0356 became 0.1245. The initial and final shapes with shaded Cp plot are shown in Figs. 4.3a – 4.3c.

5. CONCLUSIONS

A feasibility study has been conducted for using non-uniform rational B-splines and partial differential equation to represent aerospace vehicle. Unstructured grids generated by advancing front method is used to obtain surface triangulation and converged solution obtained using an Euler solver. It is seen that the surfaces produced by PDE tend to be very smooth and could accurately represent the blending of one component into another (wing into fuselage). The NURBS surface had the advantage of altering the surface by the movement of the control points. It is also noted that the PDE method could easily generate a wide variety of aerospace configurations with a slight change in the design parameter and hence is very useful in an optimization process.

Table 1. Comparison Of ADIFOR results with finite difference for geometric and nongeometric design variables.

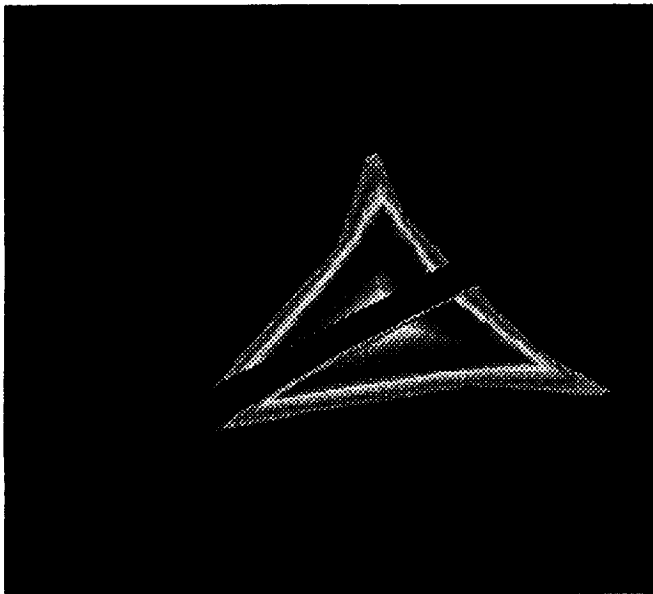|	ADIFOR		Finite Diff.	
	$\frac{\delta C_L}{\delta P}$	$\frac{\delta C_D}{\delta P}$	$\frac{\delta C_L}{\delta P}$	$\frac{\delta C_D}{\delta P}$
Angle Of Attack	0.19981	-0.21192	0.19974	-0.2127
Wing Thickness	0.171446	-0.07568	0.17146	-0.07547
Fuselage Diameter	-2.29020	-0.09421	-2.29031	-0.09420

Fig. 4.1a ADIFOR Y-coordinate sensitivity with respect to camber.
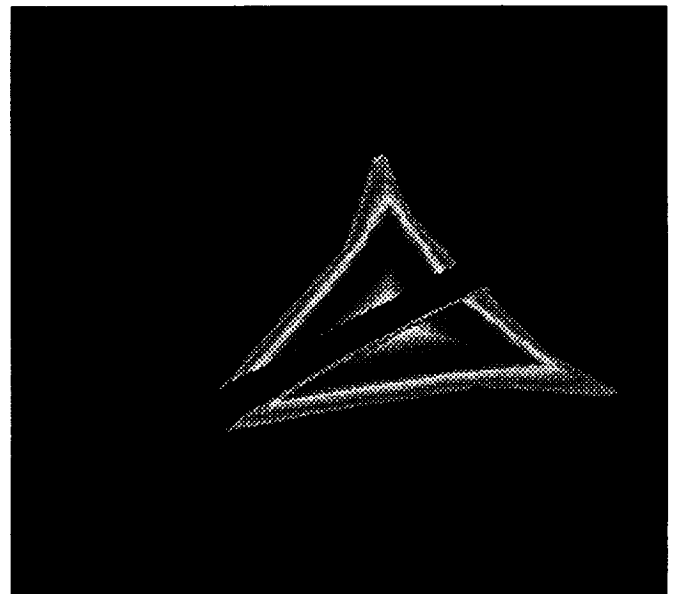

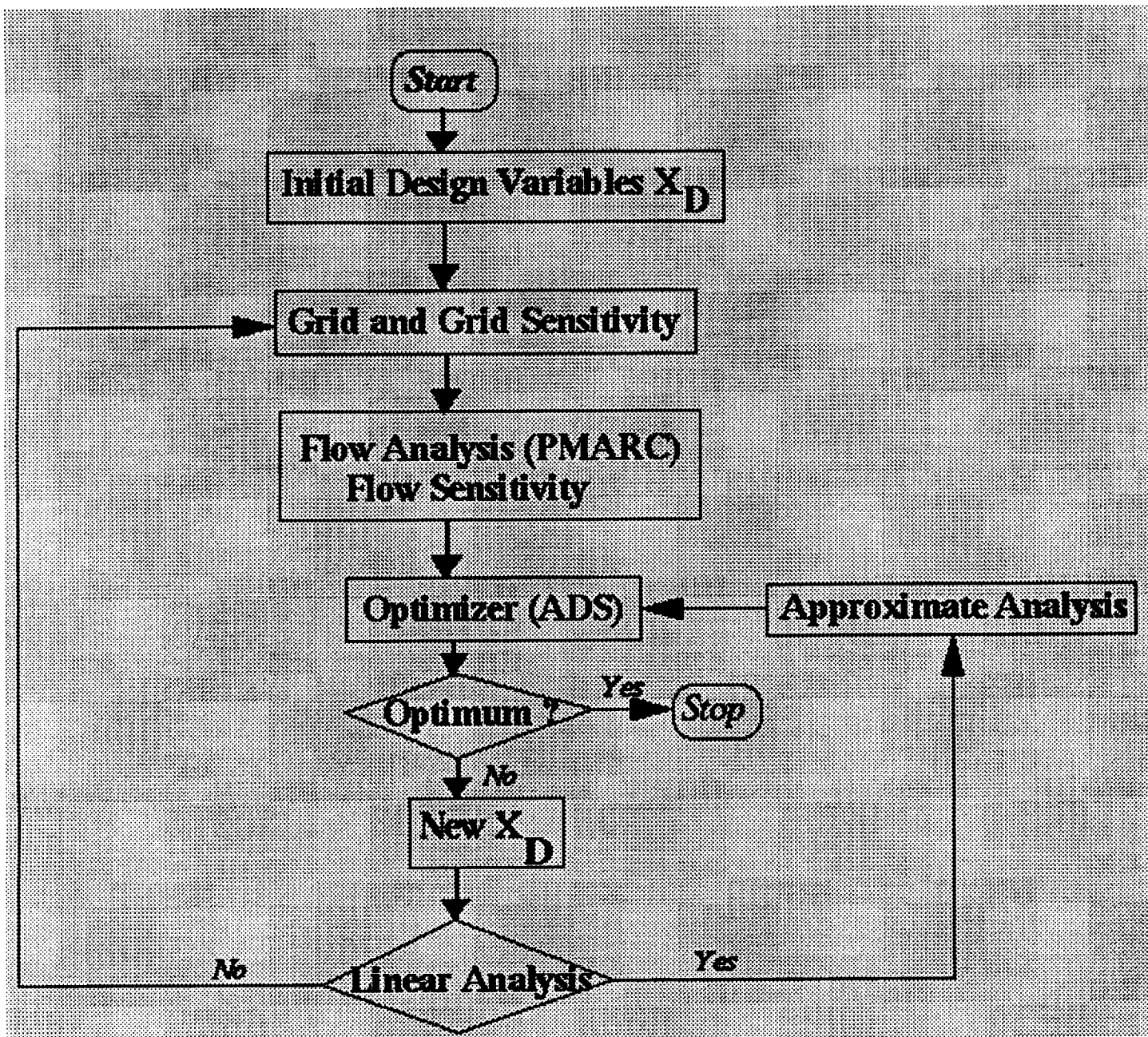**Fig. 4.1b Finite diff. Y-coordinate sensitivity with respect to camber.**
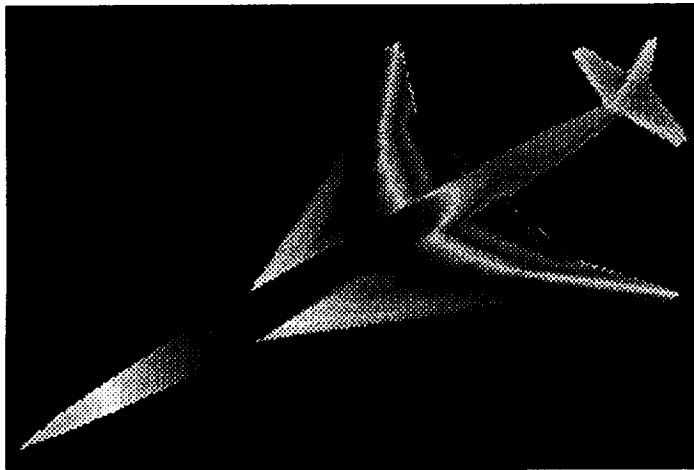
23

Fig. 4.2 Optimization Strategy Loop.
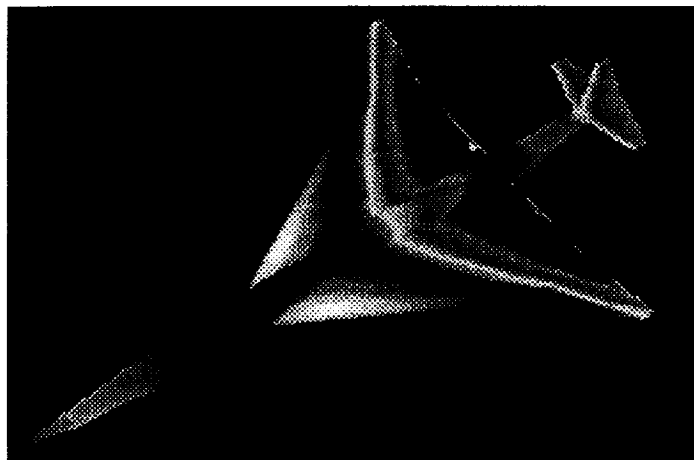
Fig. 4.3a Potential flow on the original cinfiguration.

Fig. 4.3b Potential flow on the optimized cinfiguration.
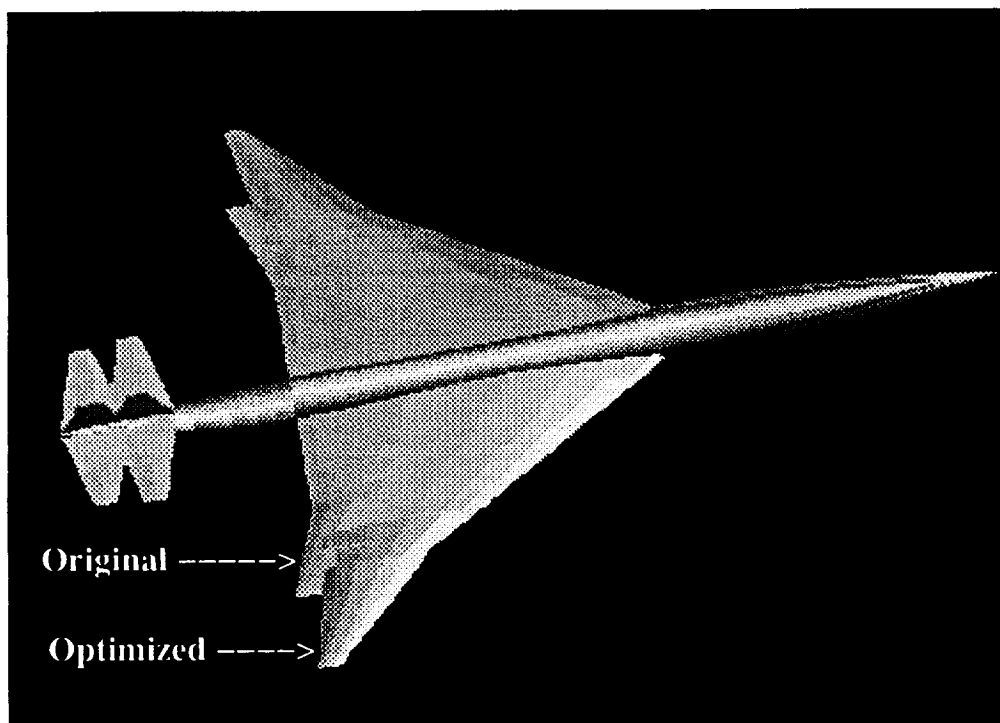

Original ----->

Optimized ----->

Fig. 4.3c Shaded plot of the original and optimized HSCT type Configuration.

6. REFERENCES

1. Thompson, J. F., Warsi, Z. U. A., and Mastin, C. W., <u>Numerical Grid Generation: Foundations and Applications</u>, North Holland, 1985.

2. IGES "Initial Graphics Exchange Specification, Version 3.0", Document No. NBSIR 86–3359, National Bureau Standards, Gaithersburg, MD, USA (1986).

3. Tiller, W. "Geometric Modelling Using Non-Uniform Rational B-Splines: Mathematical Techniques", Siggraph tutorial notes, ACM, New York, 1986.

4. Piegl, L., and Tiller, W., "Curve and Surface Construction Using Rational B-Splines", <u>Computer-Aided Design</u>, Vol. 19, No. 9, November 1987, pp. 485–498.

5. Woodward, C.D., "Skinning Techniques for Interactive B-Spline Surface Interpolation", <u>Computer-Aided Design</u>, Vol. 20, No. 8, October 1988, pp. 441–551.

6. Piegl, L., "On NURBS: A Survey", <u>IEEE Computer Graphics & Applications</u>, Vol. 11, No. 1, January 1991, pp. 55–71.

7. Bloor, M.I.G., and Wilson, M.J., "Using Partial Differential Equations to Generate Free-Form Surfaces", <u>Computer-Aided Design</u>, Vol. 22, No. 4, May 1990, pp. 202–212.

8. Bloor, M.I.G., and Wilson, M.J., "Generating Blend Surfaces using Partial Differential Equations", <u>Computer-Aided Design</u>, Vol. 21, No. 3, April 1989, pp. 165–171.

9. Bloor, M.I.G., and Wilson, M.J., "Generating PDE Surfaces in Terms of B-splines", <u>Computer-Aided Design</u>, Vol. 22, No. 6, July 1990, pp. 325–331.

10. Löhner, R., and Parikh, P., "Generation of Three-Dimensional Unstructured Grids by the Advancing Front Method", <u>International Journal of Numerical Methods Fluids</u>, Vol. 8, September 1988, pp. 1135–1149.

11. Smith, R. E., and Kerr, P. A., "Geometric Requirmets for Multidisciplinary Analysis of Aerospace-Vehicle Design", AIAA Paper No. 92–4773, September 1992.

12. Baals, D. D., Robin, A. W., and Harris, R. V., "Aerodynamic Design Integration of Supersonic Aircraft", Journal of Aircraft, Vol. 7, No. 5, September 1970, pp. 385–394.

13. Samareh-Abolhassani, J., "Unstructured grid on NURBS surfaces", AIAA Paper No. 93–3454, August 1993.

14. Frink, N. T., Parikh, P., and Piradeh, S., "A Fast Upwind Solver for the Euler Equations on Three-Dimensional Unstructured Meshes", AIAA Paper No. 91–0102, January 1991.

15. Ashby, D. L., Dudley, M. R., Iguchi, S. K., Browne, L., and Katz, J., "Potential Flow Theory and Operation Guide For the Panel Code PMARC", NASA-TM – 102851, January 1991.

16. Taylor III, A. C., Hou, G. W., and Korivi, V. M., "Methodology for Calculating Aerodynamic Sensitivity Derivatives", AIAA Journal, Vol. 30, No. 10, pp. 2411–2419, October 1992.

17. Bishof, C., Corliss, G., Green, L., Giewank, A., Haigler, K., and Newman, P., "Automatic Differentiation of Advanced CFD Codes for Multidisciplinary Design", Presented at the Symposium on High-Performance Computing for Flight Vehicles, Arlington, VA. December 1992.

18. Green, L., Newman, P., and Haigler, K., "Sensitivity Derivatives for Advanced CFD Algorithm and Viscous Modelling Parameters via Automatic Differentiation", AIAA-CP-933, AIAA 11th Computational Fluid Dynamic Conference, pp. 260–277, July 1993.

19. Vatsa, V. N., and Wedan, B. W., "Development of a Multigrid Code for 3–D Navier-Stokes Equations and its Applications to a Grid Refinement Study", Journal of Computers and Fluids, Vol. 18, pp. 391–403, 1990.

20. Thomas, A. M., Bockelie, M. J., Smith, R. E., and Tiwari, S. N., "Study on Unstructured Grid Generation Around Aerodynamic Configurations", Proceedings of the International Symposium on Scientific Computing and Mathematical Modelling, Bangalore, India, December 1992, pp. 363–399.